

# Limitation of Current Transport across the Heterojunction in Cu(In,Ga)Se<sub>2</sub> Solar Cells Prepared with Alkali Fluoride Postdeposition Treatment

Alejandra Villanueva-Tovar,\* Tim Kodalle, Christian A. Kaufmann, Rutger Schlatmann, and Reiner Klenk

Postdeposition treatments (PDTs) of chalcopyrite absorbers with alkali fluorides have contributed to improving the efficiency of corresponding solar cell devices. However, cells prepared with PDTs also tend to exhibit nonideal current–voltage ( $J$ – $V$ ) characteristics especially at low temperatures. These include blocking of the forward diode current, saturation of the open-circuit voltage with respect to temperature, a discrepancy between dark and  $J_{sc}$  ( $V_{oc}$ ) characteristics, and a crossover between dark and light  $J$ – $V$  curves. These are typical observations while measuring the temperature-dependent  $J$ – $V$  characteristics. Herein, the influence of electronic material parameters on the blocking of the current across the heterojunction in numerical simulations is reported. It is shown that a low-doped ZnO window layer, acceptor defects at the CdS/ZnO interface, or a high band offset at that interface lead to similar nonideal  $J$ – $V$  characteristics, suggesting that the carrier density in the buffer layer is a crucial parameter for the current limitation. Connections between the effects of PDT previously reported in literature and the electronic material parameters considered in the numerical model are discussed to explain the nonideal  $J$ – $V$  characteristics caused by the PDTs.

## 1. Introduction

In this contribution, we are modeling limitations of the current flow across the heterojunction in Cu(In,Ga)Se<sub>2</sub> (CIGS)-based thin-film solar cells. The study was motivated by the temperature-dependent measurement of solar cells where the absorber received an alkali fluoride postdeposition treatment (PDT). The PDT has been demonstrated to be beneficial for CIGS solar

cells. In recent years, significant improvements in chalcopyrite devices have been accomplished with efficiencies exceeding 23%.<sup>[1]</sup> This high performance was achieved by incorporating KF, RbF, or CsF into the absorber layer via PDT. Regarding the effects of alkali fluoride PDT on device parameters, an increase in the open-circuit voltage ( $V_{oc}$ ) has been observed consistently, whereas short-circuit current ( $J_{sc}$ ) and fill factor (FF) present an inconsistent trend in different contributions.<sup>[2–9]</sup> For the context of this work, we note that some publications have reported the presence of a barrier for the bucking and/or photo current, resulting for instance in a rollover of the current–voltage ( $J$ – $V$ ) characteristics or a crossover between dark and light  $J$ – $V$  curves after PDT.<sup>[7–10]</sup>


Various studies on the incorporation of alkalis can be found in the literature.

Attempts have been made to explain

changes in electronic properties and performance of the solar cell from these fundamental investigations. Studies concerning the electronic structure of the CIGS surface and CIGS/CdS interface using ultraviolet photoelectron spectroscopy (UPS) and X-ray photoelectron spectroscopy (XPS) as well as inverse photoemission spectroscopy (IPES) measurements have been given as a result of the downward shift of the valence band maximum (VBM) at the absorber surface after PDT.<sup>[11,12]</sup> Contradictory results were also reported; in the case of KF, an upward shift of the VBM<sup>[13]</sup> was derived from hard X-ray photoelectron spectroscopy (HAXPES). Similar discrepancy has also occurred while comparing the conduction band minimum (CBM) between untreated/treated PDT samples.<sup>[12]</sup> A VBM shift and/or bandgap widening at the absorber surface could reduce the interface hole concentration, and a reduced carrier recombination near the absorber surface has been assumed in previous studies.<sup>[11,14]</sup> Moreover, the downward shift of the VBM was considered as an outcome of the change of surface composition of the CIGS after PDT due to Cu and Ga depletion at the CIGS surface.<sup>[15,16]</sup> A Cu-depleted surface facilitates the in-diffusion of Cd into the copper vacancies ( $V_{Cu}$ ) during the chemical bath deposition (CBD) of the CdS buffer layer, as suggested in previous studies.<sup>[5,17,18]</sup> Therefore, the absorber surface is improved for a better buffer growth allowing a reduction of the CdS layer

A. Villanueva-Tovar, T. Kodalle, Dr. C. A. Kaufmann, Prof. R. Schlatmann, Dr. R. Klenk  
PVcomB/Helmholtz-Zentrum Berlin für Materialien und Energie  
Schwarzschildstr. 3, 12489 Berlin, Germany  
E-mail: alejandra.villanueva\_tovar@helmholtz-berlin.de

Prof. R. Schlatmann  
Hochschule für Technik und Wirtschaft Berlin  
Treskowallee 8, 10318 Berlin, Germany

 The ORCID identification number(s) for the author(s) of this article can be found under <https://doi.org/10.1002/solr.201900560>.

© 2020 The Authors. Published by WILEY-VCH Verlag GmbH & Co. KGaA, Weinheim. This is an open access article under the terms of the Creative Commons Attribution License, which permits use, distribution and reproduction in any medium, provided the original work is properly cited.

DOI: 10.1002/solr.201900560

thickness without losses in photovoltaic parameters.<sup>[10,19]</sup> According to our modeling, neither the surface bandgap widening nor the potential formation of a buried homojunction (due to Cd<sub>Cu</sub>-donors) are likely to contribute to the current limitations.

The formation of secondary phases such as RbInSe<sub>2</sub> has been described at the CIGS surface during PDT and interpreted as the layer responsible for the surface bandgap increase in the absorber.<sup>[5,20–22]</sup> As the goal here is to understand the principle mechanisms of limited current transport across the interface, no such layer has been explicitly added to the models. However, the main effects of such a layer would be a change in the band offsets and local doping which are considered in our model.

There are indications that a barrier at the back contact at least contributes to the limitation of the current transport in actual devices<sup>[23–27]</sup> in particular with PDT of the absorber.<sup>[7,10,28]</sup> Such a barrier may be needed to completely reproduce measured *J–V* curves in numerical calculations. As the emphasis here is on

**Table 1.** Device properties for a simple CIGS thin-film solar cell model used for simulations.

	p-CIGS	n-CdS	n-ZnO
Thickness [μm]	2.4	0.06	0.18
Bandgap [eV]	1.1	2.4	3.3
Electron affinity [eV]	4.4	4.3	4.45
Dielectric permittivity (relative)	13.6	10	9
CB effective density of states [cm <sup>-3</sup> ]	2.2 × 10 <sup>18</sup>	2.2 × 10 <sup>18</sup>	2.2 × 10 <sup>18</sup>
VB effective density of states [cm <sup>-3</sup> ]	1.8 × 10 <sup>19</sup>	1.8 × 10 <sup>19</sup>	1.8 × 10 <sup>19</sup>
Electron thermal velocity [cm s <sup>-1</sup> ]	1 × 10 <sup>7</sup>	1 × 10 <sup>7</sup>	1 × 10 <sup>7</sup>
Hole thermal velocity [cm s <sup>-1</sup> ]	1 × 10 <sup>7</sup>	1 × 10 <sup>7</sup>	1 × 10 <sup>7</sup>
Electron mobility [cm <sup>2</sup> V <sup>-1</sup> s <sup>-1</sup> ]	100	50	50
Hole mobility [cm <sup>2</sup> V <sup>-1</sup> s <sup>-1</sup> ]	25	25	25
Shallow uniform donor density <i>N<sub>D</sub></i> [cm <sup>-3</sup> ]	0	1 × 10 <sup>16</sup>	1 × 10 <sup>19</sup>
Shallow uniform acceptor density <i>N<sub>A</sub></i> [cm <sup>-3</sup> ]	2.5 × 10 <sup>15</sup>	0	0
Absorption constant <i>B</i> [eV <sup>(1/2)</sup> cm <sup>-1</sup> ]	1 × 10 <sup>5</sup>	1 × 10 <sup>5</sup>	From file

understanding transport across the heterojunction, the model assumes and is restricted to ideal back contact properties.

We thus focus on models with possible barriers at the hetero-interfaces of the solar cell device, considering some of the effects of RbF reported in previous studies, such as the alkali diffusion into the ZnO window layer<sup>[29,30]</sup> and the high alkali concentration near the absorber surface. Some of the nonidealities in CIGS solar cells in contrast to an ideal diode behavior are the loss in FF and the formation of a barrier for the forward diode current observed in temperature-dependent *J–V* curves (*JVT*). The modeling is conducted using SCAPS-1D simulations.<sup>[31]</sup>

## 2. Characterization and Simulation Details

For solar cell fabrication, glass substrates were coated with 800 nm-thick molybdenum followed by the deposition of the CIGS absorbers by a three-stage-based coevaporation process. There was no Na-diffusion barrier deposited on the glass, thus allowing the Na diffusion from the glass substrate into the absorber. CIGS layers were prepared with and without RbF-PDT. PDT was done in situ without breaking the vacuum, which means that the reference had to be prepared in a separate evaporation run (using the same process parameters). Subsequently, a 60 nm-thick CdS buffer layer was deposited by CBD and 40 nm-thick i-ZnO and 140 nm ZnO:Al window layers were deposited by radio frequency (RF) sputtering. Finally, Ni/Al/Ni finger grids were evaporated onto the ZnO. Process details for the respective solar cell devices can be found in the study by Kodalle et al.<sup>[7]</sup>

Measurements of the *J–V* characteristics as a function of temperature and illumination were performed in an evacuated liquid N<sub>2</sub> cooled cryostat (CryoVac) using a Keithley 2601A source measure unit in four-point configuration. The temperature range was varied from 320 to 100 K with a step size of 10 K. A solar simulator (Oriol VeraSol) with light-emitting device (LED) light sources was used to simulate the AM1.5 solar spectrum. The light intensity was varied from 100 to 0.1 mW cm<sup>-2</sup>.

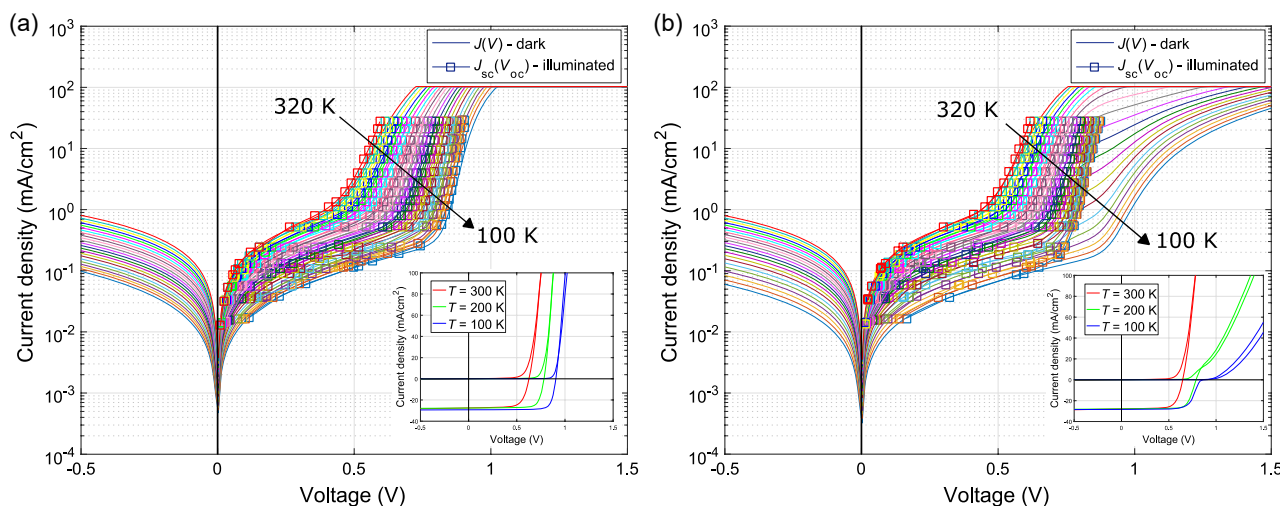


**Figure 1.** *JVT* characteristics in dark (solid lines) and under illuminated conditions (square symbols) in semilogarithmic scale of a) nontreated CIGS solar cell taken as a reference sample and b) CIGS solar cell prepared with RbF-PDT.

Numerical simulations were conducted using SCAPS-1D. The layer stack for our RbF-free reference cell consists of three layers: p-type CIGS absorber layer, n-type CdS buffer layer, and n-type ZnO window layer. Supposed beneficial effects that could result from the PDT deposition such as the increase in the carrier concentration and/or increased carrier lifetime in the absorber were neglected in the simulations, to only evaluate those effects responsible for degrading the idealities of the diode and photovoltaic performance. The parameters used for the numerical simulations are shown in **Table 1** and represent a simple model<sup>[32]</sup> with a non-graded absorber, a reasonably long diffusion length, and lifetime of charge carriers adjusted only by neutral mid-gap defects in each layer. In addition, no Fermi-level pinning and no interface defects were included in this model to avoid a change in the dominant recombination mechanism with bias overlaying the barrier effects. Conduction band alignments at the absorber/buffer and buffer/window interfaces are chosen to be a spike<sup>[33–35]</sup> and cliff,<sup>[35–37]</sup> respectively. Absorption coefficients of CIGS and CdS are set to

be high ( $B = 1 \times 10^5 \text{ cm}^{-1} \text{ eV}^{-(1/2)}$ ), whereas for ZnO, the absorption coefficient was determined via reflectance and transmission measurements as well as the reflectance of the front contact of the solar device once finished. The back contact is assumed to be ohmic (flat bands).

### 3. Results

**Figure 1** shows the temperature-dependent  $J$ - $V$  characteristics of an untreated reference CIGS sample and one treated with RbF-PDT. **Figure 1b** shows a typical example of the nonidealities that chalcopyrite thin-film solar cells exhibit when prepared with RbF-PDT, especially at low temperatures: the main effect is the blocking of the forward current at high bias voltage and low temperatures and a significant deviation between  $J_{sc}$  ( $V_{oc}$ ) values at different illumination intensities and the dark  $J$ - $V$  curves. The insets show the linear plot of dark and light  $J$ - $V$  characteristics where a slight cross-over effect can be seen at low temperatures for the PDT sample.

The activation energy ( $E_A$ ) of the saturation current can be estimated from the  $V_{oc}$  extrapolation to  $T = 0 \text{ K}$  which is shown in **Figure 2** for untreated and RbF-treated devices. A saturation of the  $V_{oc}$  can be seen at lower temperatures in both samples with a more expressed effect in the sample treated with RbF. Approximately above 200 K,  $V_{oc}$  decreases linearly with temperature. Bandgap energies were estimated from external quantum efficiency measurements obtaining  $E_g = 1.08 \text{ eV}$  and  $E_g = 1.12 \text{ eV}$  for the reference and treated sample, respectively. The  $V_{oc}$  extrapolations from **Figure 2** are approximately equal to the bandgap energy, i.e.,  $E_g \approx E_A$  in both devices, indicating that these CIGS solar cells, with or without PDT, are mainly limited by recombination in the space charge region (SCR).<sup>[38]</sup> This is another reason to limit the calculations to ideal back contact with negligible recombination. In the given example, the bandgaps are slightly different due to fluctuations in the absorber preparation and the improvement of  $V_{oc}$  and efficiency by PDT are limited. Nevertheless, the observations are typical for many pairs of cells without/with PDT that have been measured.

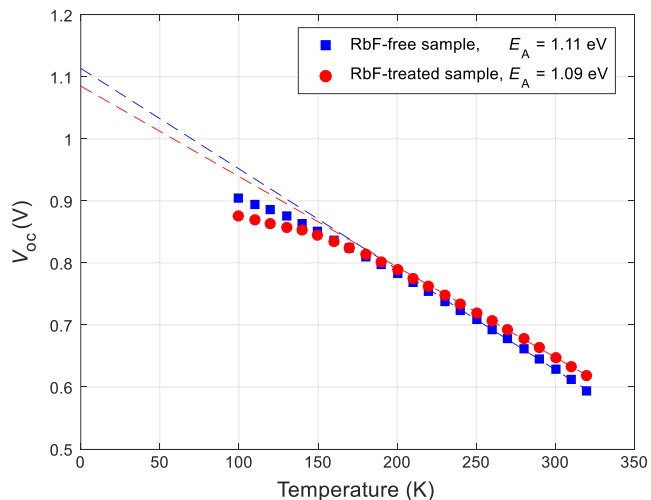


**Figure 2.**  $V_{oc}$  extrapolation to  $T = 0 \text{ K}$  for untreated and RbF-treated CIGS solar cell.

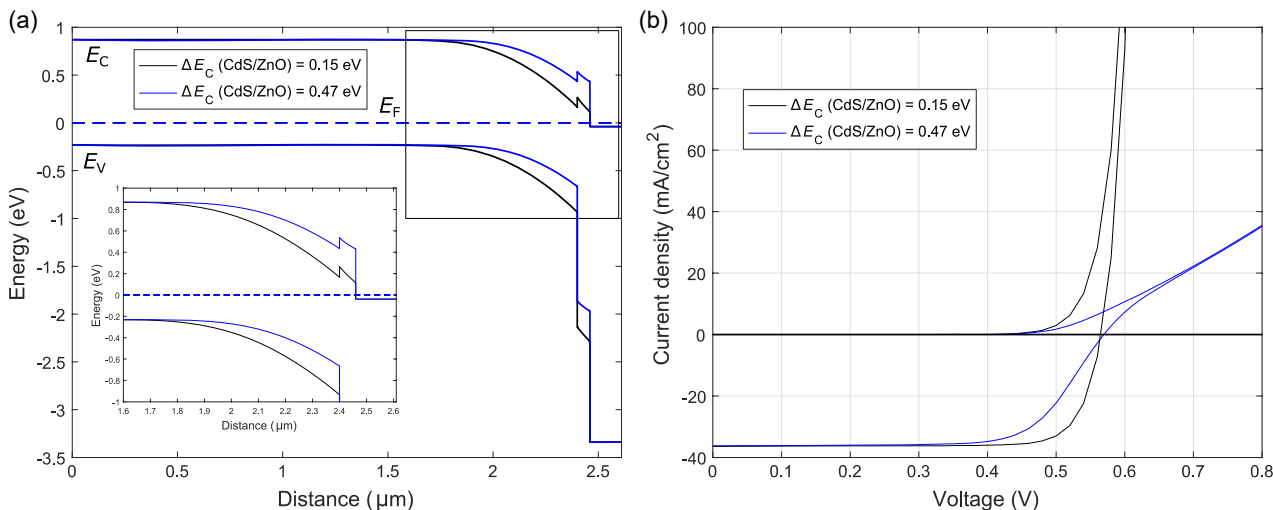


**Figure 3.** a) Equilibrium band diagram of a CIGS/CdS/ZnO thin-film solar cell. A large cliff at the CdS/ZnO interface has been introduced (blue bands). b) Simulated  $J$ - $V$  characteristics for the corresponding band diagrams where a barrier is observed for the large band offset.

To study the current limitation of the diode current at high bias voltage, a large conduction band cliff at the CdS/ZnO interface was introduced in our model (Figure 3). The main effect is the limitation of the forward diode current through the buffer layer and a poor FF, effects caused by the large separation between the CdS conduction band and the Fermi level ( $E_F$ ). The current transport through the CdS layer depends on the carrier density in the buffer layer. By increasing the band offset at the CdS/ZnO interface, the distance between the CdS conduction band and the Fermi level increases, resulting in a low charge carrier density (despite the relatively high doping, Table 1) in the buffer layer. The barrier effect emerges when the band offset of the conduction band is high enough to cause a blocking of the

forward diode current and therefore a loss in FF, in our examples, when  $\Delta E_C > 0.4$  eV. The colormap in Figure 4 shows the threshold region where the FF begins to decay with increasing band offset and decreasing ZnO doping (see the following paragraphs). In terms of doping, the ZnO layer in the model represents the i-ZnO layer in the actual device where it is located between the buffer and the highly doped ZnO:Al. The doping of the i-ZnO layer depends strongly on preparation conditions such as the oxygen partial pressure<sup>[39]</sup> during sputtering. The high doping in ZnO:Al is needed to lower the total sheet resistance but is not relevant for the current transport across the junction.

In this case of low carrier density, the electron mobility ( $\mu_n$ ) in the CdS significantly influences the current transport, as shown in Figure 5 (with a band offset at the CdS/ZnO interface of  $\Delta E_C = 0.4$  eV). While reducing the electron mobility, the barrier effect is enhanced because the transport through the CdS begins to dominate and the current scales linearly with the electron mobility when the bias voltage is greater than  $V \approx 0.6$  eV. Thus, an increased band offset at the CdS/ZnO interface (lowering the carrier density) together with a low electron mobility restricts the current transport through the buffer layer.

As the critical parameter determining the carrier density in the CdS is the conduction band position relative to the Fermi level, other parameters in addition to the band offset may be relevant. Those include the doping of the ZnO or the introduction of acceptor defects at the CdS/ZnO interface. Figure 6b shows the blocking of the forward diode current as a consequence of the three different parameters mentioned earlier. For one case, the conduction band of a low-doped ZnO layer ( $N_D = 5 \times 10^{17} \text{ cm}^{-3}$ ) is positioned above the Fermi level in an equilibrium band diagram pushing the CdS conduction band farther away from the Fermi level. However, the formation of the roll-over effect due to the ZnO doping emerges only when the conduction band offset at the CdS/ZnO interface is still considerable (Figure 4), e.g., when  $\Delta E_C = 0.4$  eV in the given example. A similar roll-over effect together with a loss in FF occurs when

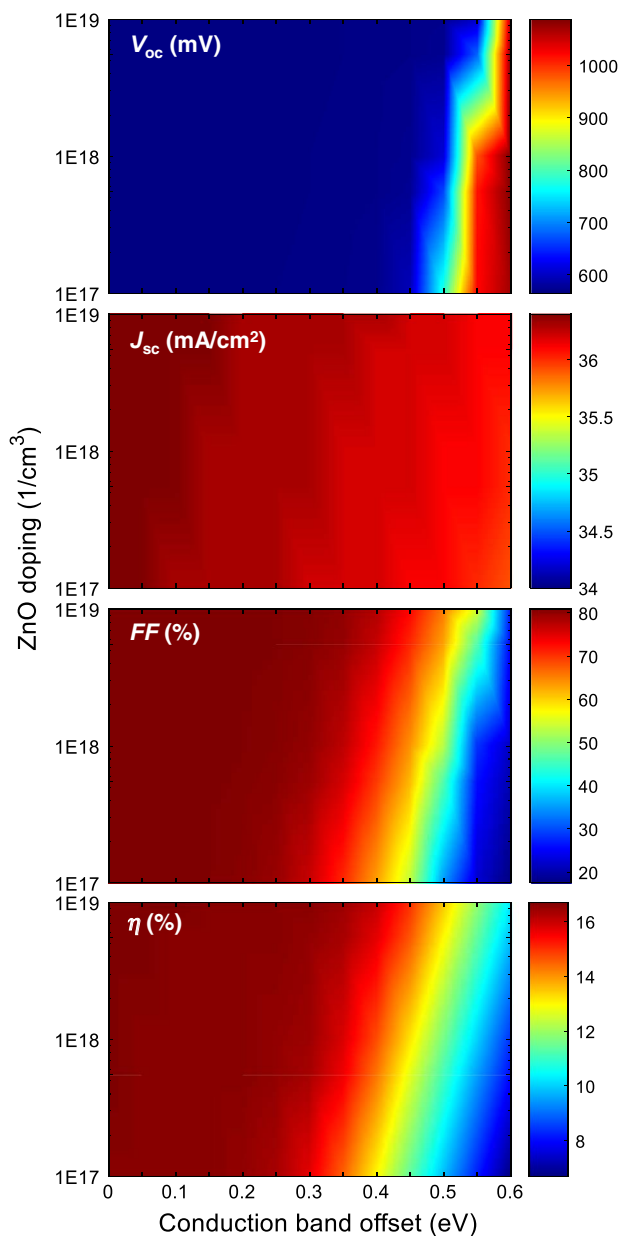


**Figure 4.** Calculated PV parameters versus ZnO doping and conduction band offset at the CdS/ZnO interface displayed on colormaps.

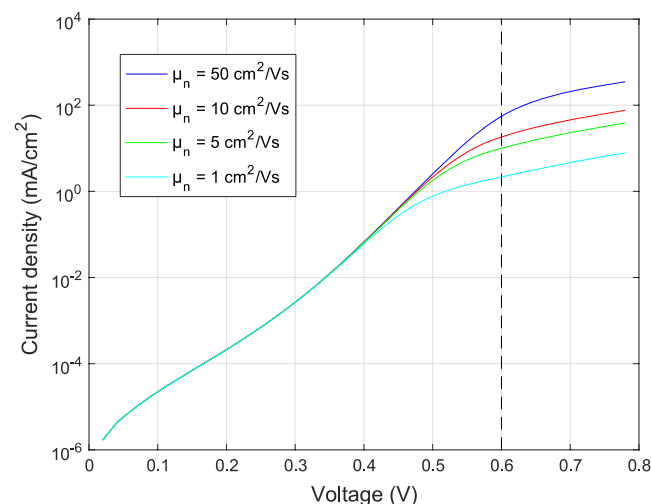


**Figure 5.** Simulated dark  $J$ - $V$  characteristics in semilogarithmic scale as a function of the electron mobility of the CdS buffer layer with a constant cliff of  $\Delta E_C$  (CdS/ZnO) = 0.4 eV.

adding acceptor defects at the CdS/ZnO interface to our reference model (Table 1). The SCR in the ZnO generated by the defects at the interface again pushes up the conduction band of the buffer layer. In summary, we can generate three band diagrams (Figure 6a), similar with respect to the CdS conduction band position, by lowering the ZnO doping (band offset of 0.4 eV), by adding defects at the interface, or by increasing the band offset to 0.47 eV, leading to comparable  $J-V$  characteristics.

In addition to the current limitation of the forward diode current as a result of a low charge carrier density of the CdS layer, a deviation at high bias voltage between  $J_{sc}(V_{oc})$  values at different illumination intensities and the dark  $J-V$  curves and a  $V_{oc}(T)$  saturation at lower temperatures were observed, and these

nonidealities are shown for the numerical calculations in **Figure 7** (only the case of defects at the interface is shown here).  $J_{sc}(V_{oc})$  points for the corresponding limited-current model are positioned on the nonblocked dark curve (Figure 7a). From this, the limited-current model seems to only affect the dark  $J-V$  characteristics without having an influence on the  $J_{sc}(V_{oc})$  points. It is evident that in such cases, it may be inappropriate to deduce diode factors from the dark  $J-V$  curves to gain information on the recombination mechanisms.

**Figure 8** shows the variations of the spike at the CIGS/CdS interface with a large constant cliff at the CdS/ZnO interface ( $\Delta E_C = 0.45$  eV). As the spike increases, the kink effect is enhanced and accompanied by a loss in FF. We note that in this

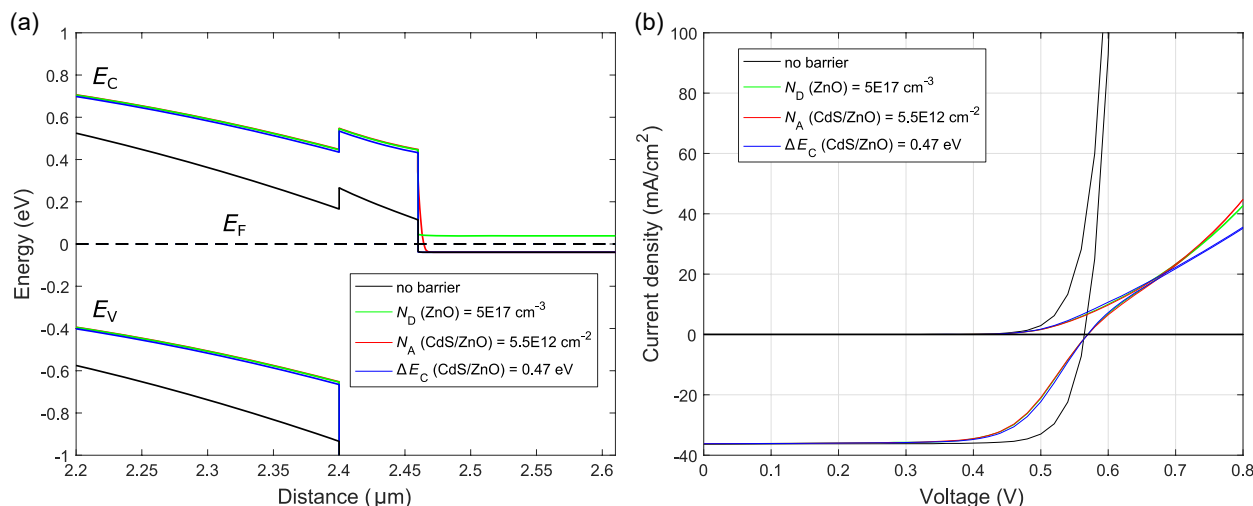


**Figure 6.** Comparison of the a) equilibrium band diagrams and b) the simulated  $J-V$  characteristics between the reference model in black color (no barrier effect with  $\Delta E_C(\text{CdS/ZnO}) = 0.15$  eV) and the three electronic material parameters modified in our model: low-doped ZnO window layer in green color ( $N_D(\text{ZnO}) = 5 \times 10^{17} \text{ cm}^{-3}$  with  $\Delta E_C(\text{CdS/ZnO}) = 0.4$  eV), acceptor defects in red color ( $N_A(\text{CdS/ZnO}) = 5.5 \times 10^{12} \text{ cm}^{-2}$  with  $\Delta E_C(\text{CdS/ZnO}) = 0.15$  eV) and high band offset at the CdS/ZnO interface in blue color ( $\Delta E_C(\text{CdS/ZnO}) = 0.47$  eV).

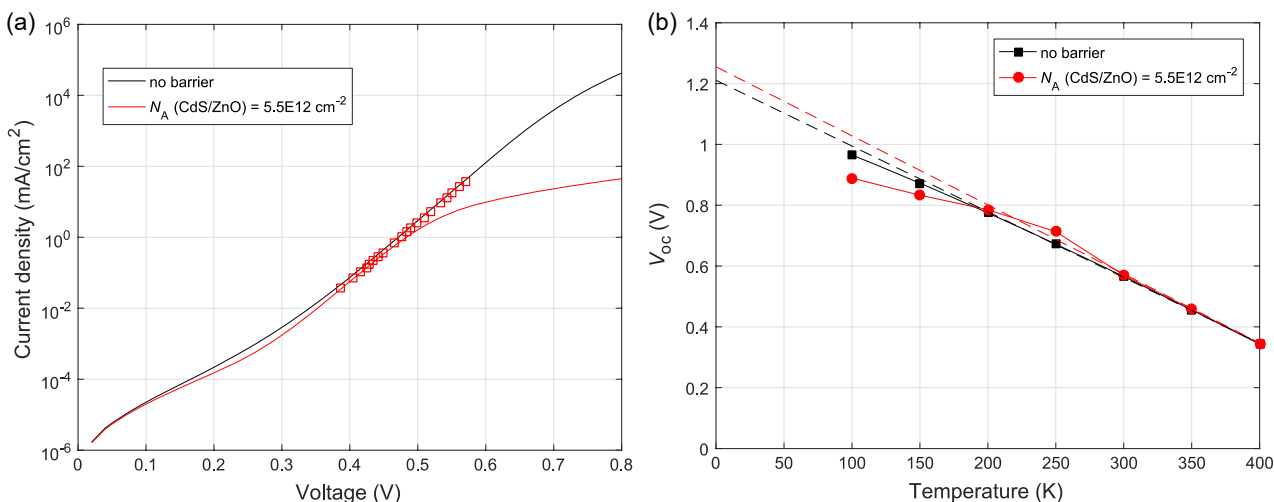


**Figure 7.** Simulated a) dark  $J-V$  characteristics in semilogarithmic scale of the reference model (no barrier effect) and the model including acceptor defects at the CdS/ZnO interface (with  $\Delta E_C(\text{CdS/ZnO}) = 0.15$  eV). Squared symbols represent the  $J_{sc}(V_{oc})$  data points for different light intensities when acceptor defects are introduced at the heterointerface; b)  $V_{oc}(T)$  characteristics including  $V_{oc}$  extrapolation to  $T = 0$  K (dashed lines).



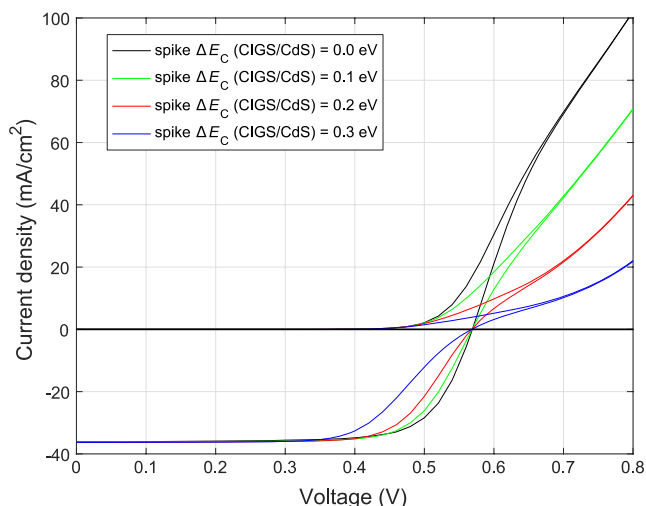


**Figure 8.** Simulated  $J$ - $V$  characteristics for different band offsets at the CIGS/CdS interface with a constant cliff of  $\Delta E_C$  (CdS/ZnO) = 0.45 eV.

combination of band offsets, the influence of the spike is noticeable earlier than in the case where only the spike is present without the cliff at the CdS/ZnO interface.<sup>[40]</sup> A higher spike can cause a reduction in the short-circuit current by creating a barrier for the transport of photogenerated carriers through the interface, as reported in previous studies.<sup>[41]</sup>

#### 4. Discussion

Our model predicts that lowering the ZnO doping, introducing acceptor defects at the CdS/ZnO interface, and/or creating a higher band offset at this interface can all contribute to lower FF, kinked  $J$ - $V$  characteristics, and a discrepancy between dark and  $J_{sc}(V_{oc})$  characteristics. This model should enable researchers who focus on material characterization to tie their results to the electronic parameters. Possible connections between the introduction of the heavy alkalis and these electronic parameters can already be suggested following the literature. Some authors have reported the in-diffusion of elements from group I into ZnO substrates. It has been demonstrated that substitutional group I elements such as Na and K introduce shallow acceptor states<sup>[29]</sup> either by diffusion or in situ during ZnO growth.<sup>[30]</sup> Based on these observations, low ZnO doping could be a consequence of Rb in-diffusion during ZnO deposition. In addition, studies demonstrated that if Na is present at the heterointerface between ZnO and CIGS in superstrate solar cells, the high density of deep acceptor states at the heterointerface lowers the FF, and therefore the device performance.<sup>[42]</sup> Notwithstanding the different preparation sequences in our substrate cells, a similar situation may nevertheless arise.<sup>[7]</sup> Thus, introducing acceptor states at the CdS/ZnO interface induced by Rb migration could explain some of the nonidealities presented in RbF-treated samples within the scope of our numerical simulations. Another consequence of alkalis and fluoride present at this interface could be the formation of dipoles and corresponding modification of the band lineup.<sup>[43]</sup>

We have shown that even a small change in the spike at the CIGS/CdS interface, when combined with the CdS/ZnO cliff, can also significantly affect the current transport. Accumulation of alkali metals and fluoride<sup>[22,44]</sup> could also change this band lineup via the formation of dipoles. A formation of an alkali-In-Se layer at the surface of the absorber after PDT<sup>[5,7,21,22]</sup> might also lead to a change in the band lineup to the buffer layer.

The effect of the incorporated Rb on the local doping level is not straightforward. It has been reported that lighter alkali elements such as Na are replaced by the heavier Rb alkali element, moving the Na from grain boundaries into grains and to the (near) surface region of the absorber.<sup>[5,7,45,46]</sup> One consequence could be a more highly doped ( $p^+$ ) layer at the absorber surface. Such a  $p^+$  layer has previously been made responsible for kinks in the  $J$ - $V$  curve.<sup>[47]</sup> It can be shown, however, that the  $p^+$  layer would mainly affect the photocurrent collection, which can explain a loss in FF but not the blocking of the dark or bucking current. The short-circuit current may be slightly reduced due to the incomplete collection and the open-circuit voltage slightly higher due to the shrinking of the SCR, but the  $J_{sc}(V_{oc})$  data points do not deviate significantly from the dark  $J$ - $V$ . In combination with the cases previously described in this contribution, the  $p^+$  layer will lead to a more severe influence on the FF.

#### 5. Conclusions

Nonidealities with respect to a standard diode are observed especially at low temperatures in temperature-dependent  $J$ - $V$  measurements of CIGS solar cells prepared with PDT. Based on numerical simulations, we have shown that in certain circumstances, the current flowing through the solar cell is limited by the transport across the buffer layer and its interfaces, and this can explain observed nonidealities. The density of carriers that is available for transport in the buffer depends on the distance between the buffer CBM and the Fermi level. This distance in turn depends on several parameters, and it was shown that increasing the band offset or the density of charged defects at the CdS/ZnO interface as well as reducing the doping of the ZnO can all result in the same depletion of carriers in the buffer. The spike at the absorber/buffer interface also influences the depletion but as it is by itself a barrier to the flow of electrons, it modifies the  $J$ - $V$  characteristics in a slightly different way. A low mobility of electrons in the buffer amplifies all nonideal effects. The clarification of the fundamental mechanism and the parameters influencing it should enable researchers that focus on material characterization to tie their results to the electronic model of the device. If the solar cell prepared without PDT is already close to the onset of current limitation, the nonideal effects can be triggered by relatively small changes in the relevant parameters. We have suggested possible connections between PDT and current transport limitations due to the migration of alkali metals. Previous studies concerning alkali PDT in CIGS solar cells have reported the in-diffusion of Rb into the ZnO window layer and at the heterointerfaces. Thus, a low-doped ZnO layer and acceptor defects at the CdS/ZnO layer might be a consequence of the alkali diffusion. A formation of interface dipoles due to alkali metals and fluoride may result

in a change in the band alignment at both interfaces. A secondary phase such as a  $\text{RbInSe}_2$  layer at the surface of the absorber might lead to a similar effect. Finally, a high Rb concentration at the absorber surface ( $p^+$  layer) is not responsible for the rollover of the  $J$ - $V$  characteristics at high bias voltage and only contributes to a greater loss in FF.

## Acknowledgements

A.V.-T. gratefully acknowledges the scholarship support from the Mexican National Council for Science and Technology (CONACYT) in cooperation with the German Academic Exchange Service (DAAD).

## Conflict of Interest

The authors declare no conflict of interest.

## Keywords

alkali fluoride postdeposition treatments,  $\text{Cu}(\text{In,Ga})\text{Se}_2$  thin-film solar cells, current transports, nonideal characteristics, numerical simulations

Received: December 12, 2019

Revised: January 23, 2020

Published online: February 10, 2020

- [1] M. Nakamura, K. Yamaguchi, Y. Kimoto, Y. Yasaki, T. Kato, H. Sugimoto, *IEEE J. Photovolt.* **2019**, 9, 1863.
- [2] S. Zahedi-Azad, R. Scheer, *Phys. Status Solidi C* **2017**, 14, 1600203.
- [3] F. Larsson, O. Donzel-Gargand, J. Keller, M. Edoff, T. Törndahl, *Sol. Energy Mater. Sol. Cells* **2018**, 183, 8.
- [4] S. Ishizuka, N. Taguchi, J. Nishinaga, Y. Kamikawa, S. Tanaka, H. Shibata, *J. Phys. Chem. C* **2018**, 122, 3809.
- [5] E. Avancini, R. Carron, T. P. Weiss, C. Andres, M. Bürki, C. Schreiner, R. Figi, Y. E. Romanyuk, S. Buecheler, A. N. Tiwari, *Chem. Mater.* **2017**, 29, 9695.
- [6] I. Khatri, K. Shudo, J. Matsuura, M. Sugiyama, T. Nakada, *Prog. Photovolt. Res. Appl.* **2018**, 26, 171.
- [7] T. Kodalle, M. D. Heinemann, D. Greiner, H. A. Yetkin, M. Klupsch, C. Li, P. A. van Aken, I. Lauer mann, R. Schlatmann, C. A. Kaufmann, *Sol. RRL* **2018**, 2, 1800156.
- [8] T. P. Weiss, S. Nishiwaki, B. Bissig, R. Carron, E. Avancini, J. Löckinger, S. Buecheler, A. N. Tiwari, *Adv. Mater. Interfaces* **2018**, 5, 1701007.
- [9] S. Ishizuka, T. Koida, N. Taguchi, S. Tanaka, P. Fons, H. Shibata, *ACS Appl. Mater. Interfaces* **2017**, 9, 31119.
- [10] F. Pianezzi, P. Reinhard, A. Chirilă, B. Bissig, S. Nishiwaki, S. Buecheler, A. N. Tiwari, *Phys. Chem. Chem. Phys.* **2014**, 16, 8843.
- [11] P. Pistor, D. Greiner, C. A. Kaufmann, S. Brunken, M. Gorgoi, A. Steigert, W. Calvet, I. Lauer mann, R. Klenk, T. Unold, M.-C. Lux-Steiner, *Appl. Phys. Lett.* **2014**, 105, 063901.
- [12] D. Hauschild, D. Kreikemeyer-Lorenzo, P. Jackson, T. Magorian Friedlmeier, D. Hariskos, F. Reinert, M. Powalla, C. Heske, L. Weinhardt, *ACS Energy Lett.* **2017**, 2, 2383.
- [13] B. Ürsür, W. Calvet, A. Steigert, I. Lauer mann, M. Gorgoi, K. Prietzel, D. Greiner, C. A. Kaufmann, T. Unold, M. C. Lux-Steiner, *Phys. Chem. Chem. Phys.* **2016**, 18, 14129.
- [14] E. Handick, P. Reinhard, J.-H. Alsmeyer, L. Köhler, F. Pianezzi, S. Krause, M. Gorgoi, E. Ikenaga, N. Koch, R. G. Wilks, S. Buecheler, A. N. Tiwari, M. Bär, *ACS Appl. Mater. Interfaces* **2015**, 7, 27414.
- [15] M. Mezher, L. M. Mansfield, K. Horsley, M. Blum, R. Wieting, L. Weinhardt, K. Ramanathan, C. Heske, *Appl. Phys. Lett.* **2017**, 111, 071601.
- [16] I. Khatri, H. Fukai, H. Yamaguchi, M. Sugiyama, T. Nakada, *Sol. Energy Mater. Sol. Cells* **2016**, 155, 280.
- [17] A. Chirilă, P. Reinhard, F. Pianezzi, P. Bloesch, A. R. Uhl, C. Fella, L. Kranz, D. Keller, C. Gretener, H. Hagendorfer, D. Jaeger, R. Erni, S. Nishiwaki, S. Buecheler, A. N. Tiwari, *Nat. Mater.* **2013**, 12, 1107.
- [18] N. Nicoara, T. Kunze, P. Jackson, D. Hariskos, R. F. Duarte, R. G. Wilks, W. Witte, M. Bär, S. Sadewasser, *ACS Appl. Mater. Interfaces* **2017**, 9, 44173.
- [19] M. A. Contreras, M. J. Romero, B. To, F. Hasoon, R. Noufi, S. Ward, K. Ramanathan, *Thin Solid Films* **2002**, 403, 204.
- [20] T. Kodalle, R. K. M. Raghupathy, T. Bertram, N. Maticiu, H. A. Yetkin, R. Gunder, R. Schlatmann, T. D. Kühne, C. A. Kaufmann, H. Mirhosseini, *Phys. Status Solidi RRL* **2019**, 13, 1800564.
- [21] N. Taguchi, S. Tanaka, S. Ishizuka, *Appl. Phys. Lett.* **2018**, 113, 113903.
- [22] N. Maticiu, T. Kodalle, J. Lauche, R. Wenisch, T. Bertram, C. A. Kaufmann, I. Lauer mann, *Thin Solid Films* **2018**, 665, 143.
- [23] T. Ott, T. Walter, T. Unold, *Thin Solid Films* **2013**, 535, 275.
- [24] T. Eisenbarth, R. Caballero, M. Nichterwitz, C. A. Kaufmann, H.-W. Schock, T. Unold, *J. Appl. Phys.* **2011**, 110, 094506.
- [25] A. Niemegeers, M. Burgelman, *J. Appl. Phys.* **1997**, 81, 2881.
- [26] A. Rockett, J. K. J. van Duren, A. Pudov, W. N. Shafarman, *Sol. Energy Mater. Sol. Cells* **2013**, 118, 141.
- [27] R. Knecht, M. S. Hammer, J. Parisi, I. Riedel, *Phys. Status Solidi A* **2013**, 210, 1392.
- [28] T. Kodalle, *Ph.D. Thesis*, Martin Luther University of Halle-Wittenberg **2020**.
- [29] C. H. Park, S. B. Zhang, S.-H. Wei, *Phys. Rev. B* **2002**, 66, 073202.
- [30] B. K. Meyer, J. Stehr, A. Hofstaetter, N. Volbers, A. Zeuner, J. Sann, *Appl. Phys. A* **2007**, 88, 119.
- [31] M. Burgelman, P. Nollet, S. Degraeve, *Thin Solid Films* **2000**, 361, 527.
- [32] M. Gloeckler, A. L. Fahrenbruch, J. R. Sites, in *Proc. of the 3rd WCPEC*, IEEE, New York **2003**, p. 491.
- [33] A. J. Nelson, S. Gebhard, A. Rockett, E. Colavita, M. Engelhardt, H. Höchst, *Phys. Rev. B* **1990**, 42, 7518.
- [34] S.-H. Wei, A. Zunger, *Appl. Phys. Lett.* **1993**, 63, 2549.
- [35] D. Schmid, M. Ruckh, H. W. Schock, *Sol. Energy Mater. Sol. Cells* **1996**, 41, 281.
- [36] A. Niemegeers, M. Burgelman, R. Herberholz, U. Rau, D. Hariskos, H.-W. Schock, *Prog. Photovolt. Res. Appl.* **1998**, 6, 407.
- [37] M. Ruck, D. Schmid, H. W. Schock, *J. Appl. Phys.* **1994**, 76, 5945.
- [38] U. Rau, *Appl. Phys. Lett.* **1999**, 74, 111.
- [39] J. P. Zhang, G. He, L. Q. Zhu, M. Liu, S. S. Pan, L. D. Zhang, *Appl. Surf. Sci.* **2007**, 253, 9414.
- [40] A. Niemegeers, M. Burgelman, A. De Vos, *Appl. Phys. Lett.* **1995**, 67, 843.
- [41] X. Zhang, Z.-K. Yuan, S. Chen, *Solar RRL* **2019**, 3, 1900057.
- [42] M. D. Heinemann, D. Greiner, T. Unold, R. Klenk, H.-W. Schock, R. Schlatmann, C. A. Kaufmann, *IEEE J. Photovolt.* **2015**, 5, 378.
- [43] R. Klausner, M. Oshima, H. Sugahara, *Phys. Rev. B* **1991**, 43, 4879.
- [44] T. Lepetit, *Ph.D. Thesis*, University of Nantes, **2015**.
- [45] P. Jackson, R. Wuerz, D. Hariskos, E. Lotter, W. Witte, M. Powalla, *Phys. Status Solidi RRL* **2016**, 10, 583.
- [46] A. Vilalta-Clemente, M. Raghuvanshi, S. Duguay, C. Castro, E. Cadel, P. Pareige, P. Jackson, R. Wuerz, D. Hariskos, W. Witte, *Appl. Phys. Lett.* **2018**, 112, 103105.
- [47] T. Walter, D. Braunger, D. Hariskos, C. Köble, H. W. Schock, in *Proc. of the 13th EU PVSEC*, WIP, Munich **1995**, p. 597.